Journal of Crystal Growth 420 (2015) 32–36

Contents lists available at ScienceDirect

Journal of Crystal Growth

journal homepage: www.elsevier.com/locate/jcrysgro

High-index Cu_2O (113) film on faceted MgO (110) by molecular beam epitaxy

Wenxing Huo [a,b], Jin'an Shi [c], Zengxia Mei [b,*], Lishu Liu [b], Junqiang Li [b], Lin Gu [c,*], Xiaolong Du [b], Qikun Xue [a,d]

[a] School of Electronic Engineering, Beijing University of Posts and Telecommunications, Beijing 100876, China
[b] Key Laboratory for Renewable Energy, Institute of Physics, Chinese Academy of Sciences, Beijing 100190, China
[c] Key Laboratory of Advanced Materials and Electron Microscopy, Institute of Physics, Chinese Academy of Sciences, Beijing 100190, China
[d] Department of Physics, Tsinghua University, Beijing 100084, China

ARTICLE INFO

Article history:
Received 29 December 2014
Received in revised form
27 February 2015
Accepted 2 March 2015
Communicated by H. Asahi
Available online 20 March 2015

Keywords:
A1. Crystal structure
A1. Reflection high-energy electron diffraction
A3. Molecular beam epitaxy
B1. Oxides
B2. Semiconducting materials

ABSTRACT

We report the growth of single-oriented Cu_2O (113) film on faceted MgO (110) substrate by radio-frequency plasma assisted molecular beam epitaxy. A MgO {100} faceted homoepitaxial layer was introduced beforehand as a template for epitaxy of Cu_2O film. The epitaxial relationship is determined to be Cu_2O (113)//MgO (110) with a tilt angle of 4.76° and Cu_2O [$1\bar{1}0$]//MgO [$1\bar{1}0$] by the combined study of in-situ reflection high-energy electron diffraction and ex-situ X-ray diffraction and transmission electron microscopy. The film demonstrates a good p-type conductivity and excellent optical properties, indicating that this unique approach is potentially applicable for high-index film preparation and device applications.

1. Introduction

Cuprous oxide (Cu_2O) is a typical p-type semiconductor with a direct band gap of 2.17 eV, which is of considerable interest due to its potential applications in photocatalytic water splitting and photovoltaic cells, as well as the possibility of realizing Bose–Einstein condensation (BEC) at relative high temperature [1]. In recent decades, various substrates have been used to fabricate Cu_2O films, such as sapphire [2,3], $SrTiO_3$ [4–7], silicon [8–11], ZnO [12–14], and MgO [15–23]. Among them MgO has attracted most attention due to its smallest lattice mismatch (~1.3%) with Cu_2O. With the lowest energy [24], Cu_2O (110) surface was found predominantly forming on MgO (001) substrate [15], and single-oriented Cu_2O (110) films on MgO (110) substrate are highly reproducible and possess a much wider growth window [23]. On the other hand, Cu_2O (001) epitaxial films were realized on MgO (001) by using plasma-assisted molecular beam epitaxy (MBE) technique [21].

In addition to the Cu_2O films with low-index surface orientations, polycrystalline Cu_2O films with a high-index (113) surface were often observed [25–28]. The Cu_2O (113) surfaces exhibit a much higher catalytic activity than the low-index surfaces, considering the fact that a higher density of atomic steps, ledges, and kinks exist in high-index surfaces [29]. It is significant, therefore, to find a route for the synthesis of single-oriented Cu_2O (113) films and investigate its optical and electrical properties as an active layer. Interestingly, Sugawara and Mae [30] have presented their findings of {100} facets on MgO (110) homoepitaxial surface when the substrate temperature was higher than 500 °C. Although in other researches single phase Cu_2O films grown on MgO (110) substrate were all (110) oriented [17–19,23], Cu_2O films on faceted MgO (110) substrate may not definitely follow the normal cube-on-cube orientations. Herein we adopted the faceted MgO (110) surface as a template for the epitaxy of Cu_2O, and finally achieved a single-oriented Cu_2O (113) film. The epitaxial relationship was investigated by the in-situ observation of reflection high-energy electron diffraction (RHEED) and ex-situ characterization of X-ray diffraction (XRD) and transmission electron microscopy (TEM). A special epitaxial relationship of Cu_2O (113)//MgO (110) is revealed, with a tilt angle of 4.76°. The in-plane orientation relationship is determined as Cu_2O [$1\bar{1}0$]//MgO [$1\bar{1}0$]. Concurrently, Cu_2O (113)

* Corresponding authors.
E-mail addresses: zxmei@iphy.ac.cn (Z. Mei), l.gu@iphy.ac.cn (L. Gu).

http://dx.doi.org/10.1016/j.jcrysgro.2015.03.021
0022-0248/

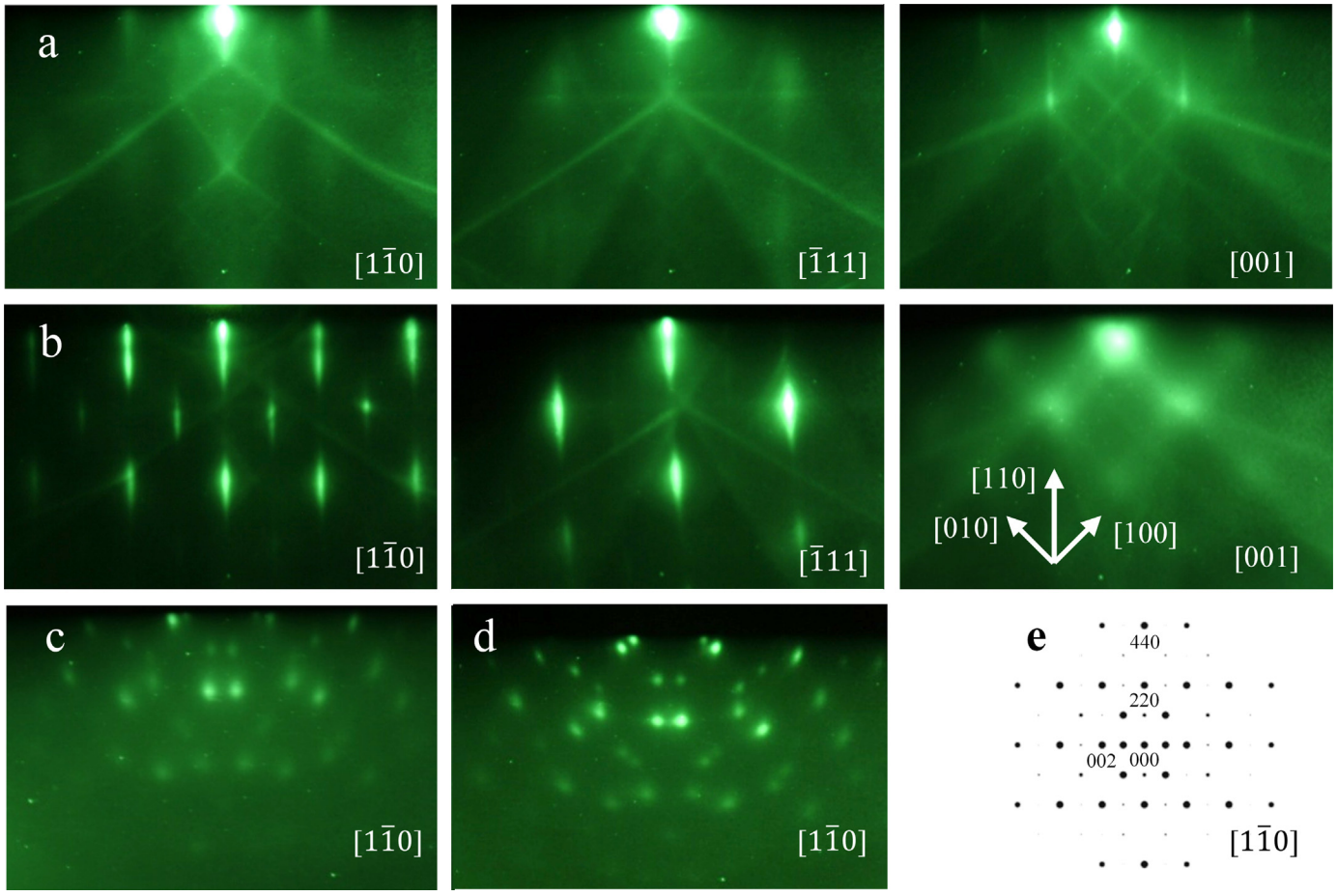

Fig. 1. RHEED patterns of (a) MgO (110) surface after loaded into the chamber and (b) MgO buffer layer with incident electron beams along [1$\bar{1}$0], [$\bar{1}$11] and [001] orientations, respectively; (c) Cu_2O buffer layer and (d) Cu_2O epilayer with incident electron beam along [1$\bar{1}$0]. (e) Simulated diagram of kinematical electron diffraction of Cu_2O with *Y* axis along [110] and zone axis along [1$\bar{1}$0].

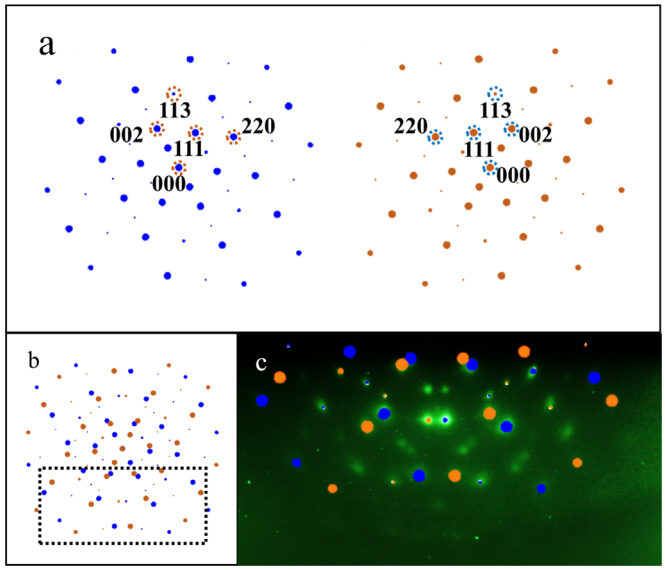

Fig. 2. (a) 60° rotation of the simulated diagram in Fig. 1 (e) and its mirror image, with spots marked by blue and orange, respectively. (b) Integrated diagram of the two diagrams in (a). (c) Fit of the RHEED pattern with the dotted box part of the integrated diagram. (For interpretation of the references to color in this figure legend, the reader is referred to the web version of this article.)

film demonstrates a good p-type conductivity and excellent optical properties, suggesting that high-index Cu_2O (113) film is promising for further device applications.

2. Experimental

Cu_2O (113) film was grown on MgO (110) single crystal substrate by using radio frequency plasma-assisted MBE (rf-MBE) technique. Elemental Cu (6 N) and Mg (5 N) were evaporated from commercial Knudsen cells while active oxygen radicals were produced by an rf-plasma source. After degreased in acetone and ethanol, the substrate was loaded into the MBE chamber and then thermally cleaned at 750 °C for 30 min, followed by oxygen plasma treatment (300 W/2.0 sccm) at 500 °C for 30 min. A homoepitaxial MgO buffer layer (~30 nm) was firstly deposited at 500 °C and subsequently annealed at 750 °C for 10 min. A regular two-step growth process was performed for Cu_2O synthesis, that is, a low temperature buffer layer grown at 500 °C for 20 min and a high temperature epilayer grown at 700 °C for 3 h. The growth conditions for both layers were kept the same, that is, Cu cell temperature of 1000 °C, rf-power of 230 W and oxygen flux of 1.0 sccm, respectively. The growth rate is ~100 nm/h, much larger than that of the Cu_2O (111) on sapphire (0001) (~50 nm/h) [2].

In situ RHEED was applied to monitor the whole growth process. Kinematical electron diffraction simulations were performed on the website of Web Electron Microscopy Applications Software (WebEMAPS, http://emaps.mrl.uiuc.edu/). XRD (Rigaku SmartLab, Cu Kα radiation, $\lambda = 1.5406$ Å) measurements were carried out to confirm the growth orientation and epitaxial relationship, which were further evidenced via TEM (JEOL-ARM200F). The surface morphology was characterized by scanning electron microscope (SEM, Hitachi 4800) and atomic force

microscopy (AFM, SIINT SPA400). Hall measurements and transmittance spectroscopy characterization were also performed to study the electrical and optical properties, respectively.

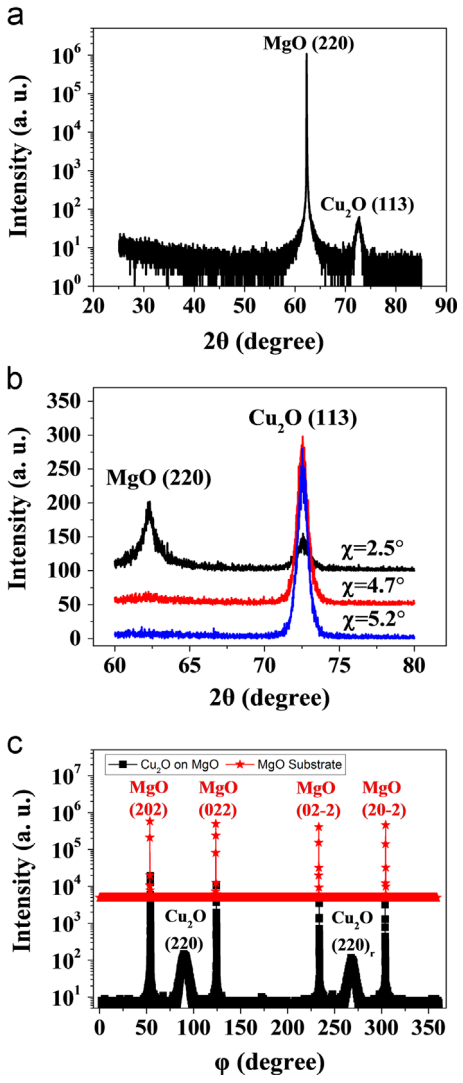

Fig. 3. XRD curves of Cu_2O film grown on MgO (110) substrate: (a) normal θ–2θ scan; (b) θ–2θ scan curves with χ varying from 2.5° to 5.2°; (c) φ scan curve with $\chi=60°$, $\theta=31.14°$ and $2\theta=62.27°$. The φ scan curve for MgO substrate with the same configurations is also presented.

3. Results and discussion

The evolution of RHEED patterns during the sample preparation process is shown in Fig. 1. Three well-defined patterns, containing distinct Kikuchi lines, are observed with incident electron beams along [1$\bar{1}$0], [$\bar{1}$11] and [001] directions of the pretreated MgO substrate [Fig. 1(a)]. The patterns along [1$\bar{1}$0] and [$\bar{1}$11] become brighter and more streaky after the homoepitaxy of MgO (110) buffer layer [Fig. 1(b)], indicating an improved crystal quality. Meanwhile, the pattern along [001] shows diffraction streaks parallel to [100] and [010], originating from the (100) and (010) facets which were well depicted in Ref. [30]. In our case, the formation of faceted MgO (110) buffer layer plays an important role in growth of high-index Cu_2O (113) film, which will be discussed later. The RHEED patterns, observed along MgO [1$\bar{1}$0], change drastically when the growth of Cu_2O starts [Fig. 1(c)], and evolve into more distinct diffraction spots with an improved contrast against the background during the rest growth process [Fig. 1(d)]. To understand these complicated patterns, we simulated the diagram of kinematical electron diffraction with zone axis along Cu_2O [1$\bar{1}$0] orientation by WebEMAPS, as shown in Fig. 1(e). Obviously, it is quite different from those patterns we observed in Fig. 1(d), indicating that the growth does not follow the commonly reported cube-on-cube orientation due to the insertion of faceted MgO (110) buffer layer.

After careful analysis, we found that the symmetric spots in present Cu_2O RHEED patterns could be divided into two groups,

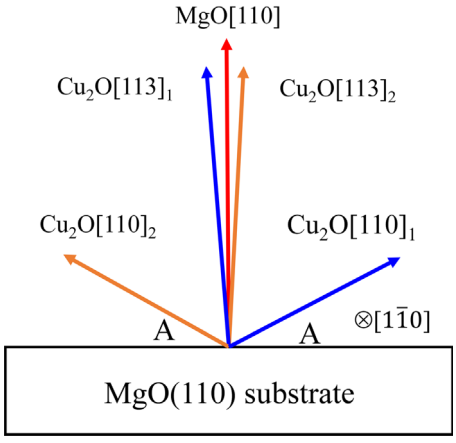

Fig. 5. Schematic of growth orientation relationship between Cu_2O (113) and MgO (110), the 180° rotation domains are marked by orange and blue arrows, respectively. The angle A is equal to 30°. (For interpretation of the references to color in this figure legend, the reader is referred to the web version of this article.)

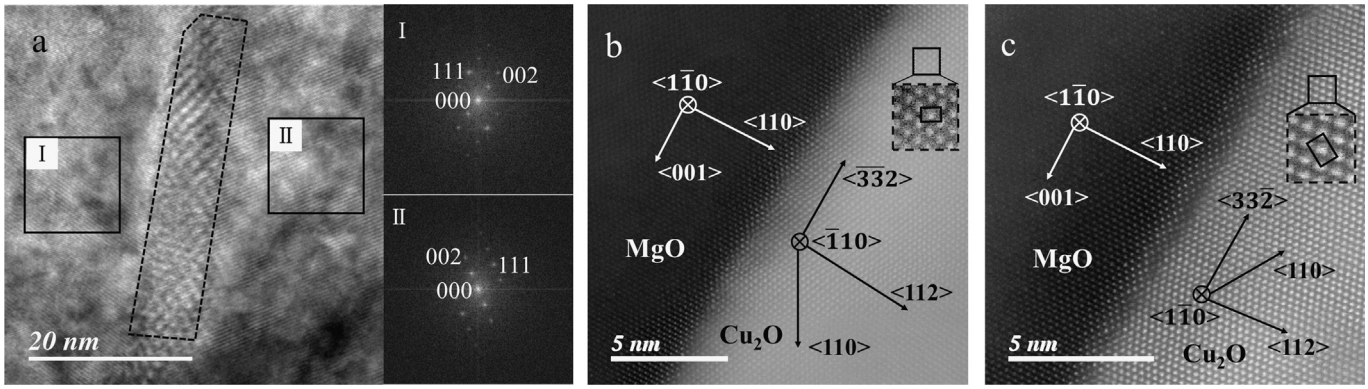

Fig. 4. (a) Cross-sectional TEM image of Cu_2O film observed along MgO [1$\bar{1}$0] orientation. The dotted polygon shows the domain boundary. (b) and (c): HAADF images of Cu_2O film on MgO in two different domains. Primitive cells were marked out by rectangles in the enlarged regions.

corresponding to two different domains. They are proved to be 180° rotated with each other, confirmed by XRD and TEM results which will be discussed below. Each group of spots occupies a rectangular lattice with an aspect ratio of $\sqrt{2}:1$, which is similar to the diagram in Fig. 1(e) except for a rotation of 60°. Hence, by rotating and mirroring, the simulated diagrams of kinematical electron diffraction for the 180° rotation domains are obtained, as shown in Fig. 2(a). Note that Cu_2O [113] is inclined at 64.76° to Cu_2O [110], so that Cu_2O [113] is close to the normal direction of substrate, namely, MgO [110]. The simulated diagrams are overlapped together and the integrated diagram is shown in Fig. 2(b). The dotted box part of the integrated diagram matches very well with the observed RHEED patterns [Fig. 2(c)], while other parts cannot be seen in RHEED due to apparatus limitation. Some spots in RHEED patterns are missing in the integrated diagram because of extinction phenomenon. Therefore, we can make a conclusion that Cu_2O [110] orientations of the 180° rotation domains are inclined at 60° to MgO [110], and Cu_2O [113] is the epitaxial orientation despite of a small tilt angle of 4.76°, which has further been confirmed by XRD and TEM analysis shown below.

XRD curves of Cu_2O film on MgO (110) substrate are shown in Fig. 3. A normal θ–2θ scan curve [Fig. 3(a)] only presents two peaks at 62.27° (denoted by Peak 1) and 72.55° (denoted by Peak 2), corresponding to the diffractions from MgO (220) and Cu_2O (113) surfaces, respectively. Peak 2 shifts approximately 1.01° from the standard 73.56° position for bulk Cu_2O (113) (ICDD PDF no. 78-2076), which is attributed to the out-of-plane expansion of the film. Here we exclude the possibility of Peak 2 originating from CuO (113) surface despite of the close peak position (72.44°, ICDD PDF no. 80-1917), as CuO phase does not exist in this epitaxial film, which has been proved by the well-defined RHEED patterns [Fig. 1(d)] and an optical bandgap of 2.54 eV (determined by the transmittance spectrum, not given here). χ-dependent (χ is a left-handed rotation about a horizontal axis) θ–2θ scans are performed to identify the tilt angle between Cu_2O [113] and MgO [110], as shown in Fig. 3(b). The intensity of Peak 1 greatly reduces when $\chi=2.5°$ and disappears when $\chi=5.2°$. Concurrently, Peak 2 achieves its maximum when $\chi=4.7°$ while Peak 1 is almost ignorable. Thus the tilt angle between Cu_2O [113] and MgO [110] is reasonably judged around 4.7°. Fig. 3(c) shows the φ scan (φ is an in-plane rotation around the center of the sample) curve of the film performed with χ, θ and 2θ fixed at 60°, 31.14° and 62.27°, respectively, while that of MgO substrate with same configuration is also presented as a reference. Two relatively broad Cu_2O (220) peaks with a 180° interval are observed, proving the existence of 180° rotation domains, which strongly supports the RHEED observations. The additional four sharp peaks have originated from MgO (202), (022), (02$\bar{2}$), and (20$\bar{2}$), respectively. Additionally, Cu_2O (220) peaks are in the middle of MgO (202) and (022) or MgO (02$\bar{2}$) and (20$\bar{2}$) peaks, indicating that the two rotation domains could be simultaneously observed along MgO [1$\bar{1}$0] orientation, which have already been observed in the RHEED patterns [Fig. 1].

Further evidences of the film orientation and microstructure by TEM are shown in Fig. 4. Cross-sectional TEM image of Cu_2O film viewed down the Cu_2O [1$\bar{1}$0] zone axis is shown in Fig. 4(a). Two regions of different domains are selected and the corresponding 2D fast Fourier transform (FFT) patterns reveal that the orientations of the two domains are rotated around the film normal axis by 180° each other, confirming again the existence of 180° rotation domains. Domain boundary marked by dotted polygon consists of some superlattice structure. The cross-sectional high-angle annular dark-field (HAADF) images show the interface of Cu_2O film and MgO substrate in two domains [Fig. 4(b) and (c)], respectively. The zone axes are along MgO [1$\bar{1}$0] orientation for both images. Primitive cells selected in the enlarged regions belong to Cu_2O {1$\bar{1}$0} surfaces, which proves that Cu_2O [1$\bar{1}$0] is parallel to MgO [1$\bar{1}$0]. Note that Cu_2O [1$\bar{1}$0] and [$\bar{1}$10] are different crystal orientations in Cu_2O (113) film, and they can equally form along MgO [1$\bar{1}$0]. That is the reason why 180° rotation domains occur in the Cu_2O (113) film. The orientation relationship is demonstrated in the images as well. As we expected, unlike the normal cube-on-cube epitaxial relationship of Cu_2O (110)//MgO (110) and Cu_2O [001]//MgO [001], Cu_2O [110] orientations are inclined at 60° to MgO [110]. Although Cu_2O [112] orientation is also close to MgO [110], the angle between Cu_2O [110] and [112] is 54.74°, so Cu_2O [112] is inclined at 5.26° to MgO [110], which is bigger than that of Cu_2O [113]. Furthermore, the atoms of Cu_2O film at the interface arrange along [33$\bar{2}$], which is vertical to [113]. The lattice mismatch between Cu_2O [1$\bar{1}$0] (3.016 Å) and MgO [1$\bar{1}$0] (2.978 Å) is 1.3%, and 15.8% between Cu_2O [33$\bar{2}$] (5.004 Å) and MgO [001] (4.213 Å). Through 6/7 domain matching, the latter could be reduced to 1.77%. Therefore, Cu_2O (113) surface can follow an epitaxy growth on MgO (110) substrate with misfit dislocations.

Given the above results, the crystal orientation and epitaxial relationship are clearly evidenced and schematically illustrated in Fig. 5. The as-grown film is confirmed to be Cu_2O (113), which is inclined at 4.76° to MgO (110) and consists of 180° rotation domains. This special growth is most likely caused by MgO {100} faceted homoepitaxial layer. In SEM and AFM characterizations, the Cu_2O (113) film manifests a grainy surface and a relatively small root mean square roughness of 9.9 nm. The film thickness is determined as ~350 nm by cross-sectional SEM image. A good p-type conductivity (hole concentration of 1.5×10^{16} cm^{-3}, mobility of 36.5 cm^2/V s and resistivity of 12 Ω cm) is attributed to the smooth and continuous film structure. The optical transmittance of the Cu_2O (113) film shows a sharp absorption edge and opacity beyond 480 nm, while the band gap E_g is deduced as 2.54 eV (not shown here). More investigations will be needed to explore the growth mechanism of high-index Cu_2O (113) film on MgO (110) substrate with {100} facets.

4. Conclusion

Single-oriented Cu_2O (113) film has been fabricated on faceted MgO (110) substrate by rf-MBE. The complicated RHEED patterns originate from the unique orientation and the existence of 180° rotation domains. XRD curves and TEM images confirm that the Cu_2O film is [113] orientated with a tilt angle of 4.76° to MgO [110], and 180° rotation domains are proved to exist in this high-index film. The smooth and continuous surface, good p-type conductivity and high transparency beyond the band gap indicate this Cu_2O (113) film can be promisingly applied in further device applications.

Acknowledgment

This work is supported by the Ministry of Science and Technology of the People's Republic of China (Grant nos. 2011CB302002 and 2011CB302006), the National Natural Science Foundation of China (Grant nos. 11174348, 51272280, 11274366, 61204067, and 61306011), and the Chinese Academy of Sciences.

References

[1] J.L. Lin, J.P. Wolfe, Phys. Rev. Lett. 71 (1993) 1222.
[2] J. Li, Z. Mei, D. Ye, H. Liang, Y. Liu, X. Du, J. Cryst. Growth 353 (2012) 63.
[3] Z. Zang, A. Nakamura, J. Temmyo, Mater. Lett. 92 (2013) 188.
[4] Y. Du, S. Atha, R. Hull, J.F. Groves, I. Lyubinetsky, D.R. Baer, Appl. Phys. Lett. 84 (2004) 5213.
[5] Z.Q. Yu, C.M. Wang, M.H. Engelhard, P. Nachimuthu, D.E. McCready, I.V. Lyubinetsky, S. Thevuthasan, Nanotechnology 18 (2007) 115601.
[6] S.V.N.T. Kuchibhatla, S.Y. Hu, Z.Q. Yu, V. Shutthanandan, Y.L. Li, P. Nachimuthu, W. Jiang, S. Thevuthasan, C.H. Henager Jr., S.K. Sundaram, Appl. Phys. Lett. 95 (2009) 053111.

[7] I. Pallecchi, E. Bellingeri, C. Bernini, L. Pellegrino, A.S. Siri, D. Marré, J. Phys. Appl. Phys. 41 (2008) 125407.
[8] J. Antony, Y. Qiang, M. Faheem, D. Meyer, D.E. McCready, M.H. Engelhard, Appl. Phys. Lett. 90 (2007) 013106.
[9] A. Chen, H. Long, X. Li, Y. Li, G. Yang, P. Lu, Vacuum 83 (2009) 927.
[10] I.S. Brandt, V. Stenger, V.C. Zoldan, J.J.S. Acuña, D.L. da Silva, A.D.C. Viegas, A.A. Pasa, Top. Catal. 54 (2011) 97.
[11] N. Gupta, R. Singh, F. Wu, J. Narayan, C. McMillen, G.F. Alapatt, K.F. Poole, S.J. Hwu, D. Sulejmanovic, M. Young, G. Teeter, H.S. Ullal, J. Mater. Res. 28 (2013) 1740.
[12] M. Izaki, T. Shinagawa, K.T. Mizuno, Y. Ida, M. Inaba, A. Tasaka, J. Phys. Appl. Phys 40 (2007) 3326.
[13] S. Jeong, E.S. Aydil, J. Vac. Sci. Technol. A 28 (2010) 1338.
[14] L.M. Wong, S.Y. Chiam, J.Q. Huang, S.J. Wang, J.S. Pan, W.K. Chim, J. Appl. Phys. 108 (2010) 033702.
[15] K. Kawaguchi, R. Kita, M. Nishiyama, T. Morishita, J. Cryst. Growth 143 (1994) 221.
[16] P.R. Markworth, X. Liu, J.Y. Dai, W. Fan, T.J. Marks, R.P.H. Chang, J. Mater. Res. 16 (2001) 2408.
[17] Z.G. Yin, H.T. Zhang, D.M. Goodner, M.J. Bedzyk, R.P.H. Chang, Y. Sun, J.B. Ketterson, Appl. Phys. Lett. 86 (2005) 061901.
[18] H. Kobayashi, T. Nakamura, N. Takahashi, Mater. Chem. Phys. 106 (2007) 292.
[19] K. Matsuzaki, K. Nomura, H. Yanagi, T. Kamiya, M. Hirano, H. Hosono, Appl. Phys. Lett. 93 (2008) 202107.
[20] W. Seiler, E. Millon, J. Perrière, R. Benzerga, C. Boulmer-Leborgne, J. Cryst. Growth 311 (2009) 3352.
[21] D.S. Darvish, H.A. Atwater, J. Cryst. Growth 319 (2011) 39.
[22] Y. Fu, H. Lei, X. Wang, D. Yan, L. Cao, G. Yao, C. Shen, L. Peng, Y. Zhao, Y. Wang, W. Wu, Appl. Surf. Sci. 273 (2013) 19.
[23] Y. Tolstova, S.S. Wilson, H.A. Atwater, J. Cryst. Growth 410 (2015) 77.
[24] A. Soon, M. Todorova, B. Delley, C. Stampfl, Phys. Rev. B 75 (2007) 125420.
[25] Y.M. Lu, C.Y. Chen, M.H. Lin, Mater. Sci. Eng. B 118 (2005) 179.
[26] S. Sung, S. Kim, K. Jo, J. Lee, J. Kim, S. Kim, K. Chai, S.J. Pearton, D.P. Norton, Y. Heo, Appl. Phys. Lett. 97 (2010) 222109.
[27] S. Wu, Z. Yin, Q. He, G. Lu, X. Zhou, H. Zhang, J. Mater. Chem. 21 (2011) 3467.
[28] Q. Huang, L. Wang, X. Bi, J. Phys. Appl. Phys. 46 (2013) 505101.
[29] Y. Liang, L. Shang, T. Bian, C. Zhou, D. Zhang, H. Yu, H. Xu, Z. Shi, T. Zhang, L.Z. Wu, C.H. Tung, CrystEngComm 14 (2012) 4431.
[30] A. Sugawara, K. Mae, Surf. Sci. 558 (2004) 211.